NASA Technical Memorandum 83056
AIAA-83-0136

Numerical Solution to the Glancing Sidewall Oblique Shock Wave/Turbulent Boundary Layer Interaction in Three Dimension

B. H. Anderson and T. J. Benson
Lewis Research Center
Cleveland, Ohio

Prepared for the
Twenty-First Aerospace Sciences Conference
sponsored by the American Institute of
Aeronautics and Astronautics
Reno, Nevada, January 10-13, 1983

NASA

Numerical Solution to the Glancing Sidewall Oblique Shock Wave/Turbulent Boundary Layer Interaction in Three-Dimension

by B. H. Anderson and T. J. Benson

National Aeronautics and Space Administration
Lewis Research Center
Cleveland, Ohio 44135

E-1521

ABSTRACT

In the present paper, some observations are made on the application of a three-dimensional viscous marching analysis (PEPSIS) to solve the glancing oblique shock wave/turbulent boundary layer interaction in three-dimensions. The experimental data of Oskam, Vas and Bogdonoff provides a description of the measured flow field and is used as the basis for an extensive benchmark verification of the 3d visicous marching analysis.

This paper delves into the solution methodology, or calculational protocol, to examine such areas as the sensitivity of initial conditions, mesh resolution, wall functions, sublayer resolution and turbulence model on the calculated results.

INTRODUCTION

The design of supersonic inlets is a difficult task in view of the wide operating range over which good performance is desired. Design of such an inlet system is strongly affected by the requirement that the aircraft operate at all speeds from zero to the supersonic design point. In addition, most supersonic aircraft must have a supersonic cruise capability where fuel economy is important. As a result of these varied and sometimes conflicting requirements, the design of a supersonic inlet is a difficult comprise.

The foregoing considerations suggest that inlet design technology would benefit from a detail and accurate flow field prediction procedure that includes shock-boundary layer interaction effects. Within rectangular inlets operating at supersonic speeds, these viscous interaction effects can be classified into three types: (1) incident shock reflections on the ramp or cowl, (2) glancing sidewall shock wave interactions, (3) corner shock wave interactions. In view of the importance of these interactions there have been a number of efforts devoted to developing, improving and implementing numerical techniques to obtain solutions to the phenomena. These solutions techniques generally fall into three categories (1) control volume methods, (refs. 1 to 3), (2) viscous marching methods, (refs. 4 to 6), and (3) Navier-Stokes solutions, (refs. 7 and 8).

In the present paper, some observations are made on the application of the viscous marching analysis (ref. 6) to the glancing oblique shock wave turbulent boundary layer interaction. An experimental study of the glancing sidewall interaction was done by Oskam, Vas and Bogdonoff (ref. 9) and provides a detailed flow description from which to verify this analysis. It is this experimental test case that forms the basis for the present study.

RESULTS AND DISCUSSION

In turbulent flows, the finite difference mesh must be packed very densely near the wall to resolve the steep velocity gradients exsisting there. This heavy packing can be partially avoided by making use of the experimentally observed properties of turbulent boundary layers. A typical unseparated boundary layer can be divided into an inner region where the total shear stress is essentially constant, and an outer region where the total shear stress decreases with distance from the wall. The inner region can be further divided into a laminar sublayer where the laminar shear stress dominates, a transition region or buffer region where both laminar and turbulent shear are important and a fully turbulent region.

When wall function boundary conditions are used, the laminar sublayer is not resolved. Rather it is assumed that the velocity near the wall obeys the law-of-the-wall and a slip or wall function boundary condition can be defined. Using wall function boundary conditions can in principle save substantial numbers of mesh points, particularly in three-dimensional flows since the near wall region is not resolved. However, in highly complex three-dimensional flows such as the glancing sidewall shock boundary layer interaction, it is not clear if this approximation will result in proper flow physics being displayed. This study, therefore, delves into the use of wall functions as well as the companion problem of the degree of mesh resolution necessary to resolve the flow physics of interest when no-slip boundary conditions are applied. Three test cases were run with PEPSIS to examine these issues. A baseline or Wall Function test case, a Coarse Mesh case with the same three-dimensional mesh as the Wall Function case but with no-slip boundary conditions and a Medium Mesh test case where the region near the tunnel sidewall was resolved. A fourth or Tunnel case was also run to demonstrate the complexity of the flow when the sidewall shock induced flow field impinges on the tunnel ceiling.

PEPSIS Computer Analysis

The PEPSIS computer code, an acronym for Parabolic Elliptic Streamwise Implicit Supersonic, was developed jointly by NASA Lewis Research Center and Scientific Research Associates. It is a fully three-dimensional computer design code for supersonic inlets. The computer analysis possess the general three-dimensional viscous nature of the Navier-Stokes equations, but takes advantage of realistic physical approximations to limit computer run time and storage requirements associated with the solution of the complete three-dimensional Navier-Stokes equations. The assumption is made that a "primary" flow direction exists and that diffusion arising from the rate of change of the flow in this "primary direction" can be neglected. In this manner a set of steady state equations is produced for entirely supersonic flows which are solved by an efficient spatial marching procedure.

Glancing Sidewall Shock Wave Interaction

A schematic diagram depicting the analytical and experimental test configuration used to study the glancing sidewall shock wave boundary layer interaction is shown in figure 1. This interaction arises when the oblique shock wave formed by the wedge interacts with the boundary layer exsisting along the tunnel wall. This interaction is fully three-dimensional since the

position of the shock on the tunnel wall surface changes in the cross stream direction. Because of the skewing of the incident shock on the tunnel wall, a strong transverse gradient produces a cross flow with the tunnel wall boundary layer in a direction along the shock wave. Downstream of the shock wave, the transverse static pressure gradient disappears. At a given distance normal to the tunnel sidewall within the boundary layer interaction zone, the flow properties vary rapidly in the direction normal to the tunnel sidewall. While the region of study in the experimental investigation was confined primarily to the center section of the tunnel sidewall, the analytical study includes the ramp surface, the corner region and the tunnel sidewall.

Figure 2 shows the shock generator along with the experimental survey planes, which were the same in the analysis for the purpose of data comparisons. The streamwise coordinate X was measured from the leading edge of the wedge, the normal coordinate Y was measured relative to the wedge surface and the coordinate Z was normal to the X-Y plane. For this study, the wedge angle was set at 10.0°.

Calculational Test Conditions

The coordinate system and represented computational mesh used in this study are depicted in figure 3 along with the identification of important surfaces critical to this calculation. These important surfaces include the initial data plane, located upsteam of the ramp tip, the ramp surface and the tunnel sidewall. Also shown on figure 3 is the inviscid location of the shock generated by the 10.0° wedge. The analysis of the glancing sidewall shock wave boundary layer interaction was started upstream of the wedge tip in the initial plane. The nominal free stream Mach number at this upstream location was set at 2.94, the tunnel total pressure was set at 88.9 psia and the tunnel free stream total temperature was 445.0° Rankine. This gave a free stream average operating Reynolds number of 1.28E6, based on a reference length of 0.667 feet. The tunnel sidewall turbulent boundary layer in the initial plane was sized to match the measured profiles at the reference survey plane at X = 3.5 inches using a Maise-McDonald initial boundary layer profile (ref. 11). This gave a boundary layer thickness of 0.55 inches upstream of the interaction which was assumed to be uniform across the entire tunnel sidewall.

Boundary Conditions and Turbulence Model

The PEPSIS computer analysis used for this study has the provision to independently prescibe separate boundary condition on each of the bounding surfaces of the computational domain represented in figure 3. In each of the four test cases reported in this paper, the McDonald-Camarata turbulence model (ref. 11) was applied to all wall surfaces and wall function boundary conditions were prescribed on the ramp surface downstream of the ramp tip. Upstream of the ramp tip, the streamwise component of velocity was held fixed. In the region of the ramp tip, the wall function boundary conditions were applied using an obstacle logic procedure developed by Buggeln (ref. 6) in order to minimize the computational problems associated with the leading edge ramp tip singularity. Along the tunnel sidewall, two types of wall boundary conditions were studied. The baseline Wall Function case applied wall function boundary conditions to each of the bounding surfaces. In addition to this Wall Function case, two additional case were studied using no slip boundary conditions along the tunnel sidewall. The Coarse Mesh case used the identical

computational mesh as the Wall Function baseline case where the yplus of the first grid point off the tunnel sidewall was 271. This placed the first mesh point off the tunnel sidewall outside the laminar sublayer. A Medium Mesh case was also studied in which the mesh points were packed normal to the tunnel sidewall such that the first mesh point away from this wall was at a yplus of 71, which is marginally outside the laminar sublayer. To maintain the same resolution in the outer region of the flow field, the number of mesh points normal to the sidewall was increased from 40 to 60. Since only half the tunnel was considered in this analysis, symmetry boundary conditions were applied on the surface passing through the tunnel centerline. To save mesh points and consequently to reduce the overall computer run time, symmetry boundary conditions were also applied on the surface represented by the tunnel ceiling. This boundary condition was later changed to a wall function boundary condition i.e. Tunnel test case, to study the influence of the boundary layer developing along the tunnel ceiling and to examine the effect of the impinging glancing sidewall shock wave interaction. To perform this calculation, the number of mesh points normal to the ramp surface was increased from 40 to 80 to resolve the tunnel ceiling boundary layer.

The PEPSIS computer design code also has the input option of implementing either constant enthalpystagnation flow conditions or computing the static and total temperature field by using the full energy equation. For the series of calculations to be presented, constant stagnation enthalpy conditions were employed.

Computational Mesh and Run Time

A summary of the test cases showing the mesh and computing time on both the IBM 370/3033 and CRAY I is presented in table I. The two computing times listed under the IBM 370/3033 computer represent two operating modes of the NASA Lewis Computing System. With an Internal Symbol Dictonary (ISD), computations can be performed in an interactive mode. This allows the user to directly interact with the computation of the problem while the code is in core. When this option is removed, the computing time is reduced by about 40 percent for the PEPSIS computer code. While the test cases listed in table I were not actually run on the CRAY I computer, the times listed are estimated from PEPSIS cases that have been run. The CRAY I computing time listed does not represent a fully optimized compter code for this machine, and much work is planned in this area. In general, the computing times shown in table I are highly competitive in this stage of development of the PEPSIS computer design code.

Calculated Results and Comparison with Experimental Data

Pitot pressure - The predicted pitot pressure distribution at the reference survey plane X = 3.5 inches is compared with the measured data for the five rake positions in figures 4 and 5. Figure 4 presents a comparison between the Wall Function and Coarse Mesh test cases while figure 5 shows the effects of mesh resolution by comparing the Coarse and Medium Mesh test cases. As can be seen in both figures 4 and 5, a discrepancy between data and the analytical prediction can occur because of insufficent mesh resolution in the near wall region when no-slip conditions are applied. Both the wall function results, figure 4, and the medium mesh no-slip results, figure 5, provide very good agreement with the pitot pressure data upstream of the sidewall interaction. While the initial data applied was sized to match the

boundary layer thickness at this reference plane, it becomes quite clear that even in a region with no substantial pressure gradient, discrepancies an arise with no slip with insufficient near wall resolution. Figures 5, 6 and 7 present the same study but in a region where large transverse static pressure gradients exist as a result of the interaction of the shock wave with the tunnel sidewall boundary layer. The predictions of pitot pressure when wall function boundary conditions were applied at the tunnel sidewall show remarkable agreement with data, figure 5. However, even with moderate near wall resolution as represented by the Medium Mesh test case, a discrepancy occured in the near corner region between the ramp and tunnel sidewall surfaces. The differences between the analytical prediction and experimental data may be due to any of several possibilities, the most likely being insufficient mesh resolution in the near corner region. This suggests that to properly resolve the global flow field in this interaction, the small length scales associated with the corner flows may have to be resolved. It should also be pointed out that the near wall and near corner regions are very difficult to experimentally survey and every effort should be made to obtain accurate data.

Static pressure - The predicted static pressure distribution as obtained by using both wall functions and no-slip boundary conditions are presented in figures 9, 10 and 11 and compared with the measured data at the rake survey planes located at X = 5.1 and X = 7.6 inches. In general, excellent agreement with the static pressure data was achieved for all the types of applied boundary conditions considered in this paper. This suggests that the static pressure prediction is not as sensitive to insufficient near wall resolution as the total pressure. The largest discrepancy occured at the rake survey plane when the shock wave was well outside the boundary layer and in the free stream, YG = 2.75 inches, figure 11. This was caused by the lack of mesh resolution in the outer portion of the flow field.

Figure 12 presents the static pressure signatures calculated on the ramp surface and tunnel sidewall. Also shown is a schematic diagram of the complete tunnel configuration showing the location and orientation of the wedge and resulting shock wave. The numerical formation of the shock wave in the region of the wedge tip can clearly be observed as well as the shock wave on the tunnel sidewall surface. Although not explicitly shown in figure 12, an adverse pressure gradient exsists in the near wall region of the wedge surface and tunnel sidewall which was measured in (ref. 9). Of special interest also is the fact that static pressure gradients are established on the ramp surface as a result of the corner flow boundary layer development and that the maximum static pressure on the ramp surface occurs just away from the tunnel sidewall causing low energy fluid to flow in towards the corner region.

Yaw angle - The yaw angle is defined as the ratio of the velocity in the YG-direction which is parallel to the tunnel sidewall, divided by the velocity in the X-direction, see figures 2 and 3. This is a particularly difficult parameter to calculate and measure since it represents the ratio of two velocities which approach zero as the wall is approached. Therefore, it would be expected to be the most sensitive and the most difficult flow variable to match with experimental data.

Shown in figures 13 and 14 are the effects of applying wall function boundary conditions along the tunnel sidewall, figure 13, and the effects of increasing mesh resolution in the near wall region, figure 14. Both these comparisons were performed at the X = 5.1 inch survey plane location. In general, both the wall function and medium mesh calculational results showed excellent agreement with the experimental data, although the wall function

results are somewhat lower than the measured results. Excellent agreement was also obtained at rake survey planes of X = 7.1 inches, figure 15 and the survey plane X = 7.6 inches, figure 16, for the Medium mesh calculational results. Of interest is the fact that the calculated and measured yaw angle increased in the downstream direction, figures 14 to 16, and eventually exceed the inviscid shock wave angle, YG = 1.75 through 3.00 inches in figure 16. It is also quite apparent that insufficient resolution of the near wall region when no-slip boundary conditions are applied caused discrepancies to occur in the calculation of the velocity field of this interaction.

Flow Field Visualization

A detailed picture of the flow field in the tunnel sidewall region is shown in figure 17. The computed secondary velocity shown are relative to the computational mesh shown in figure 3. In the vicinity of the tunnel sidewall, a very strong vortex is established which elongates and increases in strength in the downstream direction. This causes very low energy fluid to accumulate in the corner region with resulting low wall shear stress in this region. This probably accounts for the the very high heating rates measured by Cskam, Vas and Bogdonoff (ref. 9). The increasing strength of the sidewall vortex is also suggested by the experimental data results since the maximum yaw angle increases in the downstream direction, as can be seen in figures 14 to 16. The very rapid formation of this sidewall vortex is illustrated in figure 18, where the the wedge leading edge region was magnified to illustrate this formation. The overturning that occurs in the sidewall boundary layer results from an imposition of the main stream static pressure gradient upon the low momentum near wall viscous flow. This overturning results in low energy fluid being drawn in towards the tunnel sidewall in the lower ramp region. In the outer ramp region, the flow rolls over to form the sidewall vortex. The surface velocity vectors, i.e., the velocity vector at the first mesh point off the wall is presented in figure 19. As the flow develops in the downstream direction, the surface velocity vectors tend to align themselves with the shock angle. The shear stress signature that results from this secondary flow structure is shown in figure 20. The lowest wall shear stress occurs in the near corner region of the wedge surface and tunnel sidewall intersection. Also shown in figure 20 is a schematic diagram of the tunnel configuration showing the orientation of the wedge and the resulting inviscid shock wave.

Complete Tunnel Calculation

Of particular importance in the design of two dimensional supersonic inlets is the effect of the sidewall vortex system when it impinges on the tunnel ceiling and how best to control this interaction. To obtain some insights into this benchmark interaction, a fourth or Tunnel test case was run where the ceiling boundary layer was also resolved. Figure 21 presents the results of this calculation in the form of secondary velocity vectors. At station 92, the flow is such that the corner just begins to react to the sidewall vortex system. The shock wave in the outer portion of the flow field shown has not come into view. By station 98, the original shock wave appears in the outer region and the corner flow begins the shock wave reflection process. Although the static pressure rise is not sufficient to separate the flow on the center portion of the tunnel ceiling, the flow begins to separate within the corner region causing a strong shock wave to develope. This

shock wave propagates into the outer region in a diagonal direction as can be seen between stations 101 through 116. Thus a highly three-dimensional reflected shock wave develops which separates the flow in the corner region. Unpublished experimental data obtained in the 1x1 ft. Supersonic Wind Tunnel at Lewis Research Center for similar conditions confirms the existence of this separated region.

CONCLUSIONS

This paper describes a numerical solution to the glancing sidewall oblique shock wave turbulent boundary layer interaction in three-dimensions by a supersonic spatial forward marching computer design code PEPSIS. A test case was run to investigate the use of the wall function boundary condition approximation for a highly complex three-dimensional shock boundary layer interaction. In general, very good results were obtained with the wall function condition boundary approximation. Two additional test cases were run to examine the question of near wall resolution when no-slip boundary conditions are used. In the Coarse Mesh test case, the first mesh point off the wall was at a yplus of 271.0, while for the Medium Mesh case, the yplus was 71.0. The yplus for this latter case was marginally close to the laminar sublayer and showed substantially better comparision with experimental data, particularly the yaw angle data. The differences between the Medium Mesh numerical results and experimental data occur in the pitot pressure distribution in the near corner region of the flow field. While these differences could be due to any of several possibilities, the most likely is insufficient mesh resolution in the near corner region. This suggests that to properly resolve the global flow field, the small lengths scales associated with the flow in the near corner region may also have to be resolved. The resulting flow field was such that a strong sidewall vortex was established which elongated and increased in strength in the downstream direction. This vortex system caused low energy fluid to accumulate in the corner region resulting in very low wall shear stress. When this sidewall vortex system impinged on the tunnel ceiling surface, the flow in the corner separated and formed a highly three-dimensional shock wave system which propagate out in a diagonal direction.

In general, the PEPSIS computer design code gave excellent results compared with the sidewall shock wave turbulent boundary layer interaction data of Oskam, Vas and Bogdonoff. Although much work is planned to improve the fluid flow physics, generalize the geometry and decrease the computing time by conversion and optimization on the CRAY I computer, it is self evident that the PEPSIS compter code is practical for three-dimensional supersonic inlet calculations.

REFERENCES

1. Fukuda, M. K., Hingst, W. R. and Reshokto, E., "Control of Shock Wave-Boundary Layer Development in a Mach 2.5 Mixed Compression Inlet," NASA TM X-2060, April 1974.
2. Hingst, W. R., and Towne, C. E., "Comparison of Theoretical and Experimental Boundary Layer Development in a Mach 2.5 Mixer Compression Inlet," NASA TM X-2026, April 1974.
3. Paynter, G. C., "Analysis of Weak Glancing Shock/Boundary Layer Interactions," AIAA Paper 79-0144, January, 1979.
4. Buggeln, R. C., McDonald, H., Kreskorsky, T. D. and Levy, R., "Development of a Three-Dimensional Supersonic Inlet Flow Analysis," NASA CR-3218, November, 1979.

5. Anderson, B. H., and Towne, C. E., "Numerical Simulation of Supersonic Inlets Using a Three-Dimensional Viscous Marching Viscous Analysis," NASA TM-81411, January, 1980.
6. Buggeln, R. C., McDonald, H. and Kin, Y. W., "Computation of Multi-Dimensional Viscous Supersonic Flow by Spatial Forward Marching," AIAA Paper No. 83-0177, January 1983.
7. Shang, J. S., Hankey, W. L. Jr, and Law, C. H., "Numerical Simulation of Shock Wave-Turbulent Boundary Layer Interaction," AIAA Journal, Vol. 14, Oct. 1979.
8. Knight, D. D.: "Improved Numerical Simulation of High Speed Inlets Using the Navier-Stokes Equations," AIAA paper No. 80-0383, 1980.
9. Oskam, B., Vas , I. E., and Bogdonoff, S. M., "Mach 3.0 Oblique Shock Wave/Turbulent Boundary Layer Interactions in Three-Dimensions," AIAA Paper No. 76-336.
10. McDonald, H., and Camarata, F. J., "An Extended Mixing Length Approach for Computing the Turbulent Boundary-Layer Development," In Procedings Stanford Conference om Computation of Turbulent Boundary Layers, Vol. I, published by Stanford University, 1069, pp 83-98.
11. Maise, G. and McDonald, H., "Mixing Length and Kinematic Eddy Viscousity in a Compressiblle Boundary Layer", AIAA Journal, Vol. 6, No. 1, January 1968, pp 73-79.

TABLE I. - TEST CASES, MESH AND COMPUTING TIME

CASE	MESH	COMPUTING TIME (MIN)		
		IBM 370/3033		CRAY 1#
		ISD	NO ISD	
WALL FUNCTION	40x40x120 (192 000)	53.1	62.0	7.2
COARSE MESH YPLUS=271	40x40x100 (160 000)	44.0	26.0	6.0
MEDIUM MESH YPLUS=71	40x60x90 (216 000)	60.0	36.0	9.6
TUNNEL	80x40x120 (384 000)	104.0	62.0	14.4

#ESTIMATED TIME

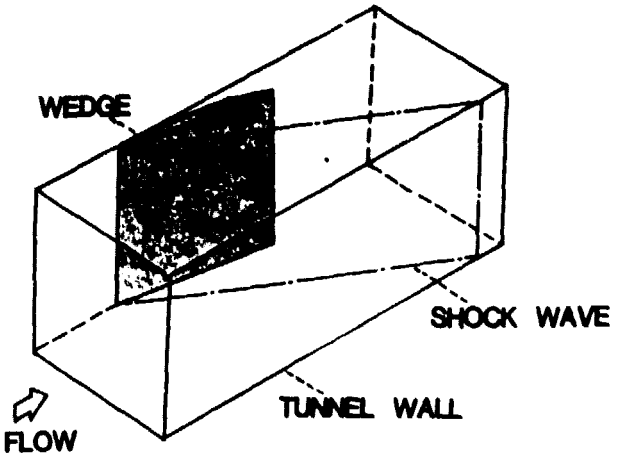

Figure 1. - Schematic diagram of the computational/experimental test configuration.

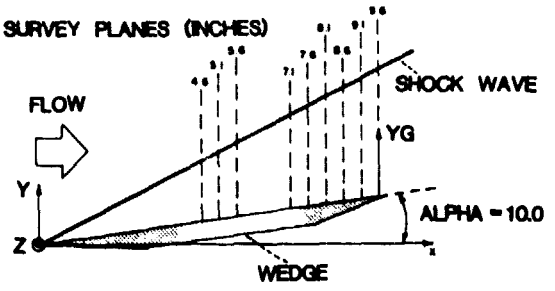

Figure 2. - Experimental survey planes.

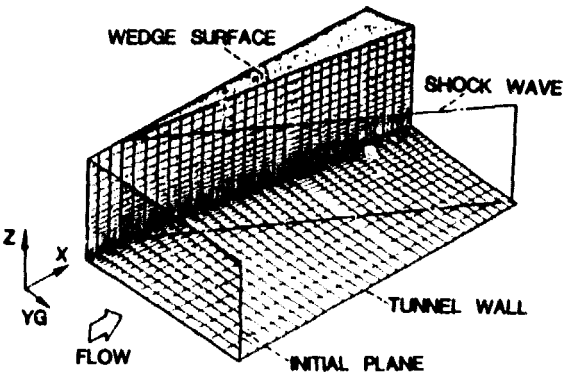

Figure 3. - Coordinate system and computational mesh.

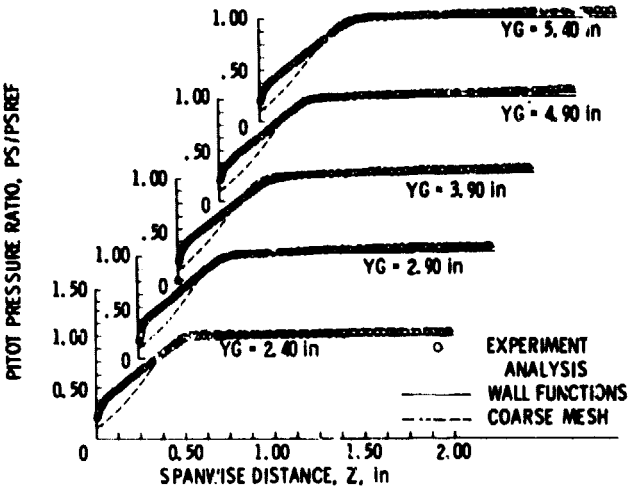

Figure 4. - Effect of wall functions on the pitot pressure distribution in the reference survey plane, X = 3.6 in.

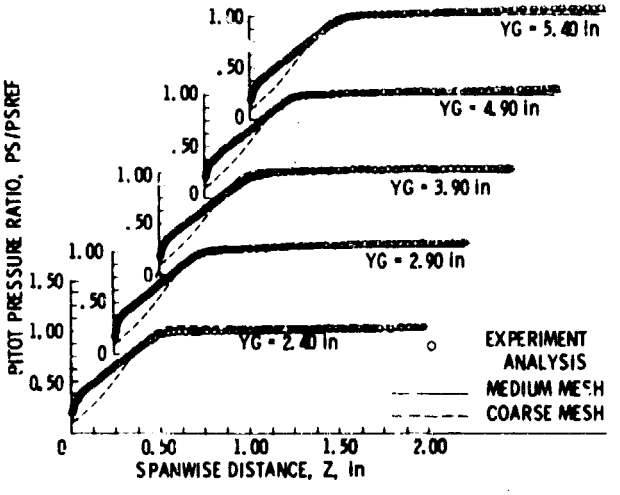

Figure 5. - Effect of mesh resolution on the pitot pressure distribution in the reference survey plane, X = 3.6 in.

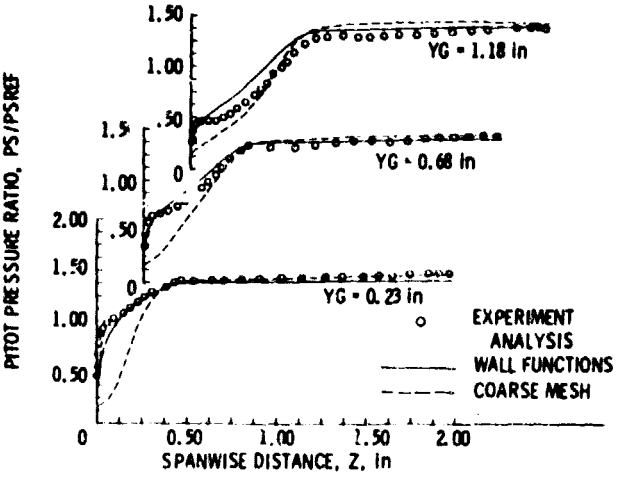

Figure 6. - Effect of wall functions on the pitot pressure distribution in the survey plane X = 5.1 in.

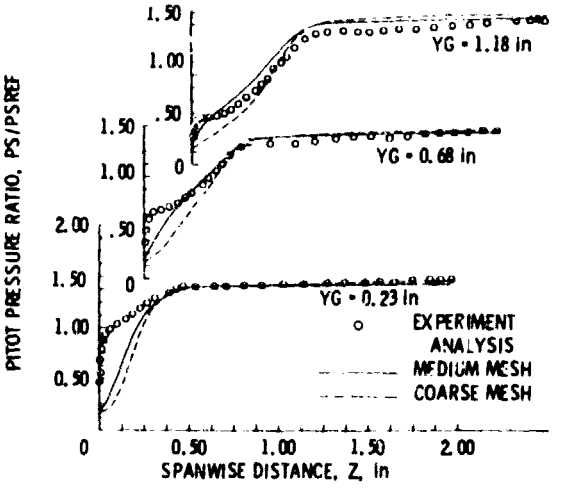

Figure 7. - Effect of mesh resolution on the pitot pressure distribution in the survey plane X = 5.1 in.

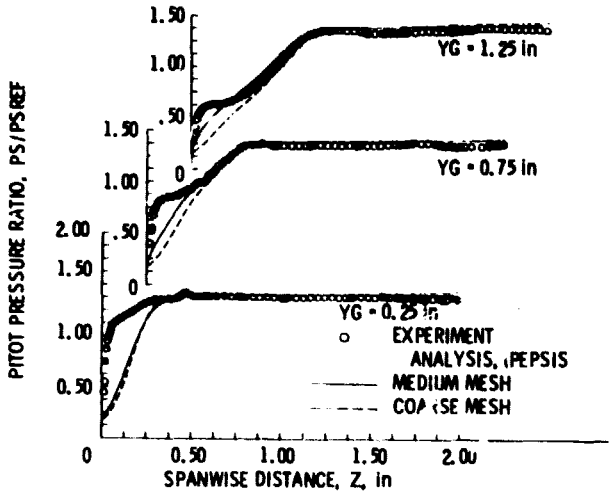

Figure 8. - Effect of mesh resolution on the pitot pressure distribution in the survey plane X = 7.1 in.

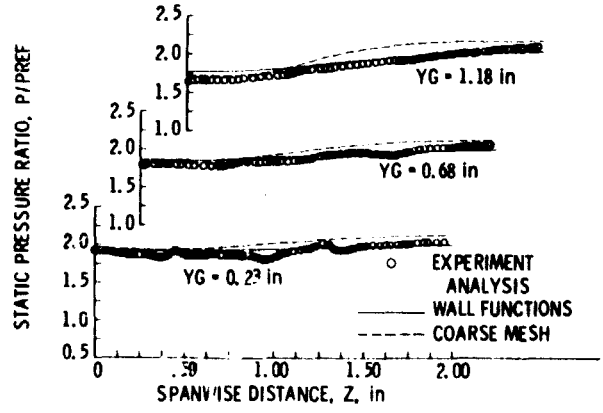

Figure 9. - Effect of wall functions on the static pressure distribution in the survey plane X = 5.1 in.

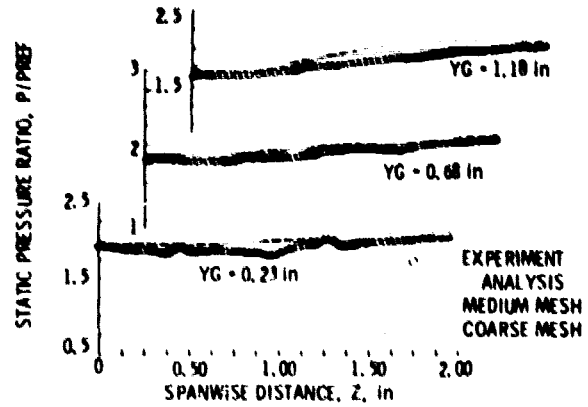

Figure 10. - Effect of mesh resolution on static pressure in the survey plane X = 5.1 in.

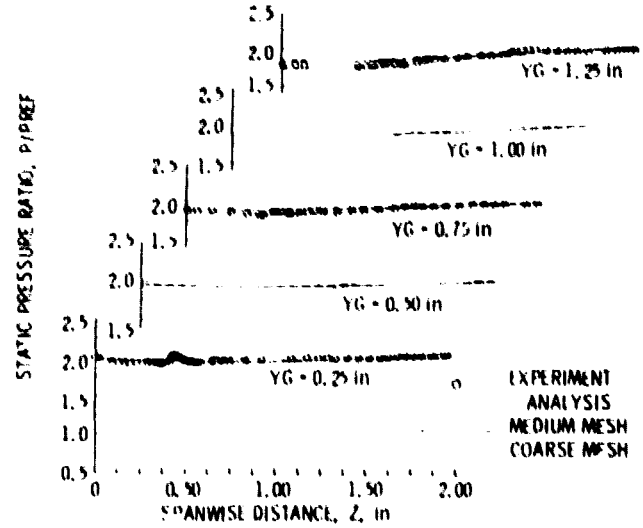

Figure 11. - Effect of mesh resolution on the static pressure distribution in the survey plane X = 7.6 in.

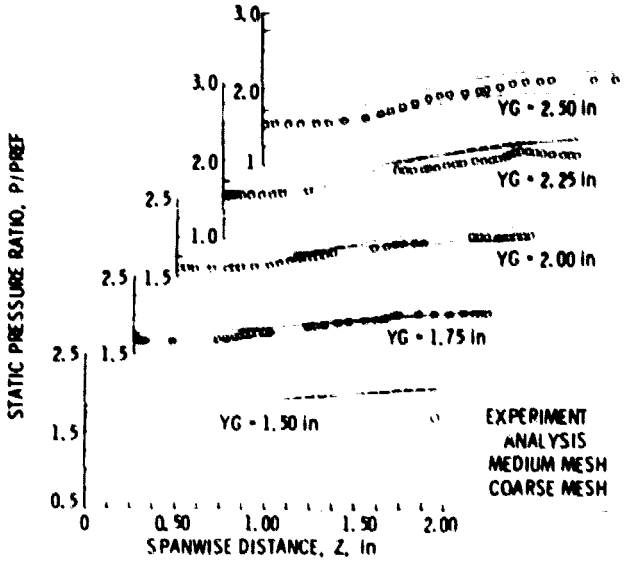

Figure 11. - Continued.

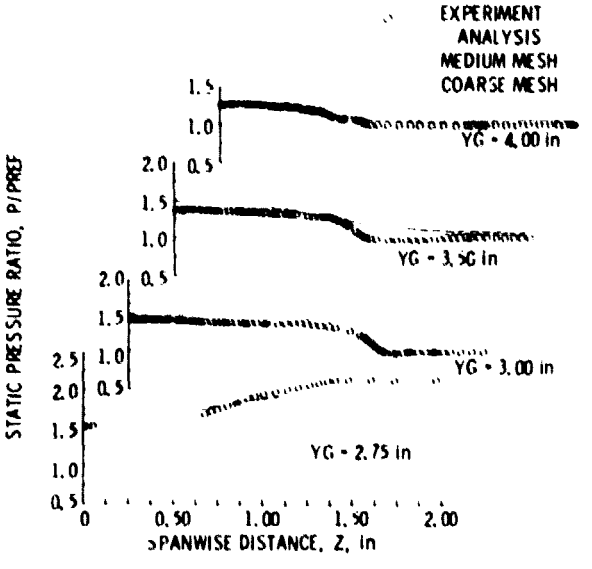

Figure 11. - Concluded.

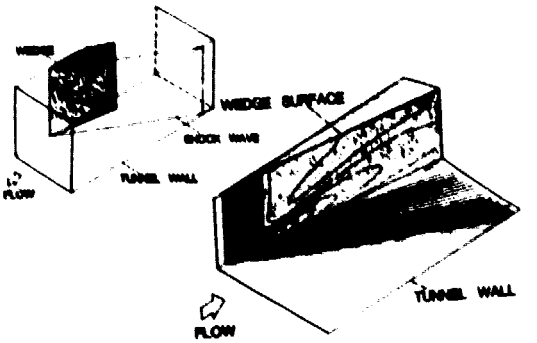

Figure 12. - Static pressure signatures on the ramp surface and tunnel wall.

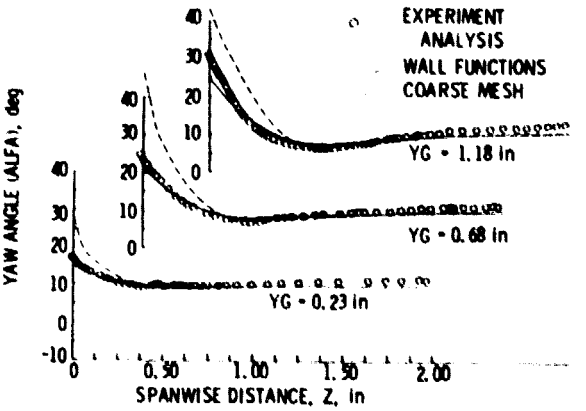

Figure 13. - Effect of wall functions on the yaw angle distribution in the survey plane X = 5.1 in.

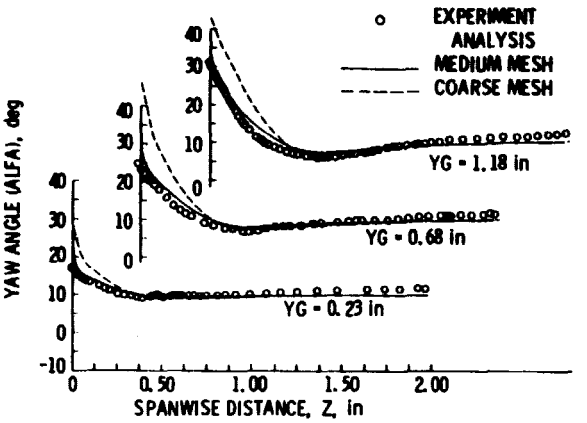

Figure 14. - Effect of mesh resolution on the yaw angle distribution in the survey plane X = 5.1 in.

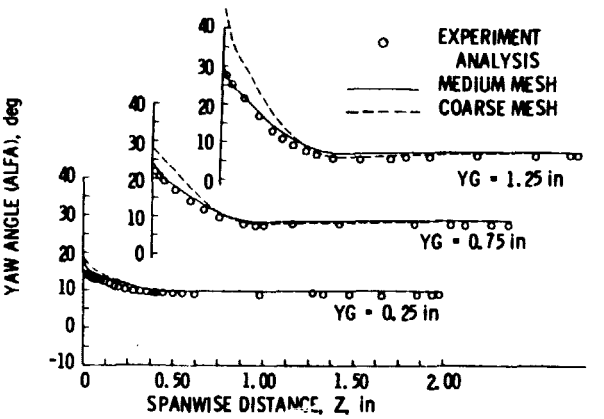

Figure 15. - Effect of mesh resolution on the yaw angle distribution in the survey plane X = 7.1 in.

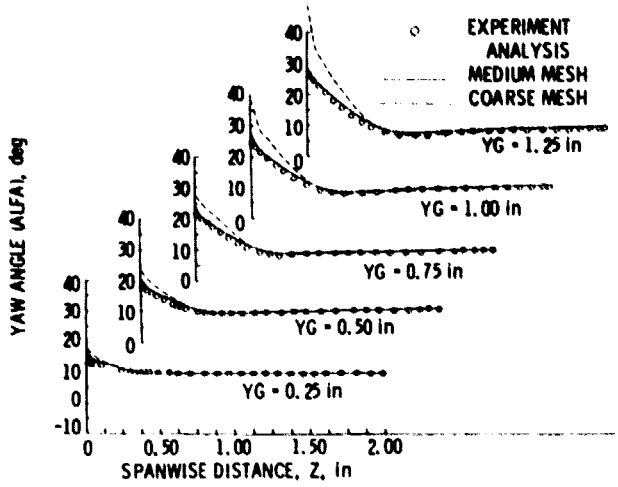

Figure 16. - Effect of mesh resolution on the yew angle distribution in the survey plane X = 7.6 in.

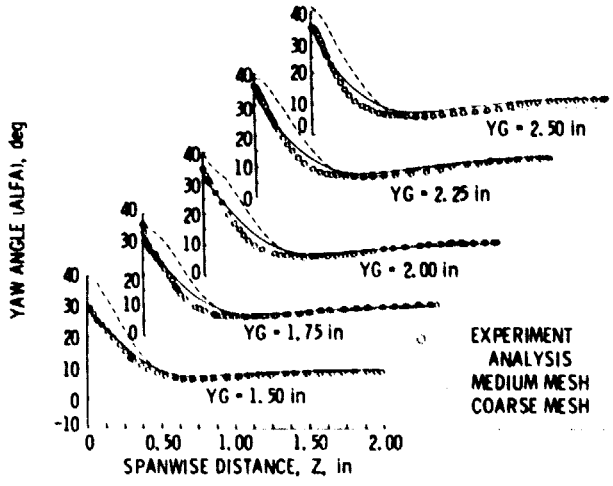

Figure 16. - Continued

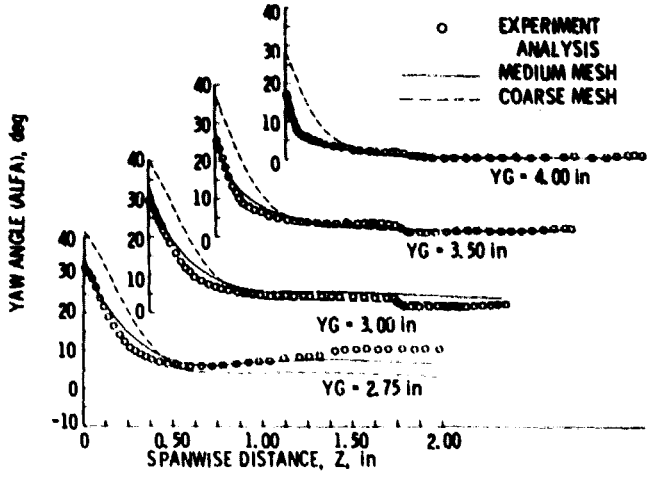

Figure 16. - Concluded.

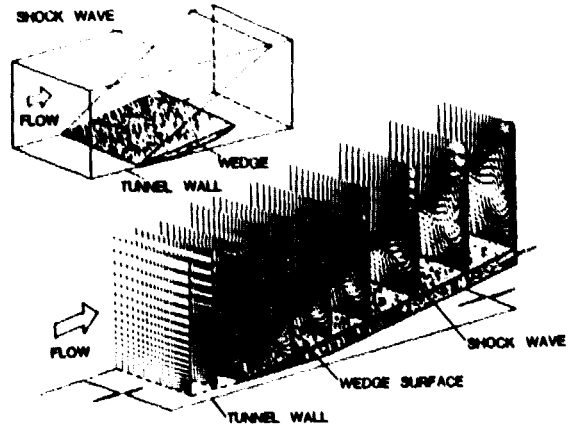

Figure 17. - Sidewall vortex formed by the glancing shock wave boundary layer interaction.

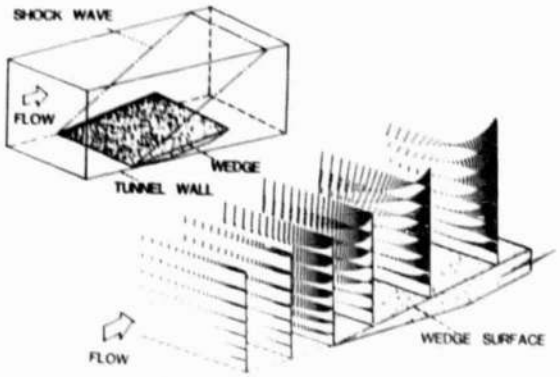

Figure 18. - Formation of the sidewall vortex.

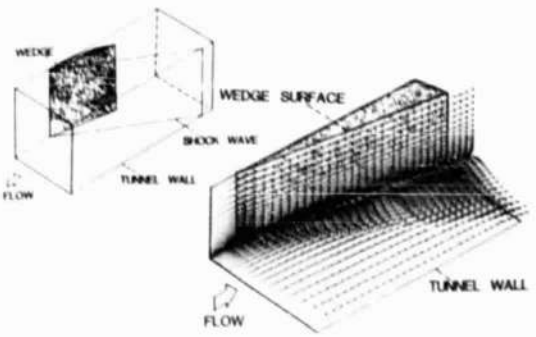

Figure 19. - Surface velocity vectors.

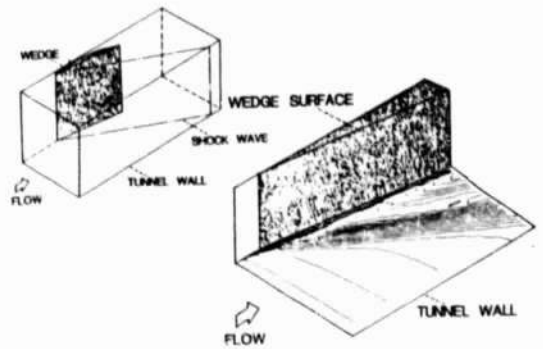

Figure 20. - Shear stress signature on the tunnel wall.

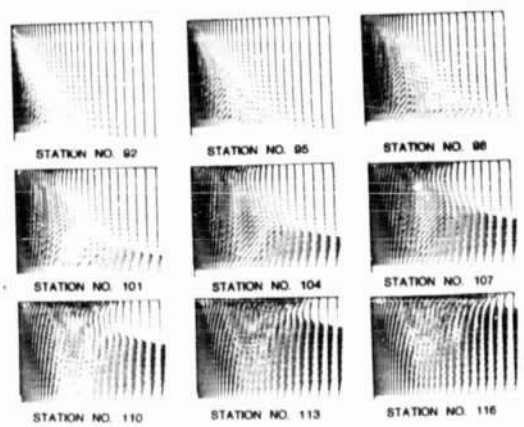

Figure 21. - Impingment of the sidewall vortex on the tunnel ceiling.